Mon. Not. R. Astron. Soc. **000**, 000–000 (0000) Printed 28 June 2017 (MN LATEX style file v2.2)

Galaxy Zoo Hubble: the passive disk fraction decreases from $z = 1.0$ to $z = 0.3$ or maybe increases who even knows

Melanie A. Galloway[1],several others

[1]*School of Physics and Astronomy, University of Minnesota, 116 Church St. SE, Minneapolis, MN 55455, USA*

28 June 2017

ABSTRACT

1 INTRODUCTION

It is well known that most galaxies tend to exist in one of two populations: blue, late-type disks exhibiting active star formation, and red, early-type ellipticals showing little to no signs of recent star formation (Strateva et al. 2001; Baldry et al. 2004; Correa et al. 2017). The division between the two color populations is quite distinct when visually represented on a color-magnitude or color-color diagram. Galaxies tend to populate in one of two regions: the "red sequence" in the upper band, which contains predominently early-type galaxies, and the "blue cloud" in the lower, containing mostly late-type spirals. This bimodality in the color-morphology relationship of galaxies has been so widely accepted that color is often used as a proxy for morphological classification in large samples of galaxies (e.g. Cooray (2005); Lee & Pen (2007); Salimbeni et al. (2008); Simon et al. (2009)), where expert visual classification is not feasable on such scales, while measurements of colors are readily available.

The relatively tight correlation suggests an evolutionary link between a galaxy's dynamical history (traced by its morphology) and stellar content (traced by its color). In the simplest interpretation, it could be deduced that galaxies tend to begin their lives as young, star-forming disks, until some mechanism (secular or external) causes star-formation to cease while the galaxy simultaneously undergoes a morphological tranformation from disk to spheroidal.

The advent of larger surveys and more reliable methods for measuring morphology (independently of color) has allowed for more nuanced interpretations of the simple model. For instance, the degree of incompleteness in the color-morphology relationship is now much more realized, with the recent identifcations of significantly large samples of red spirals and blue ellipticals. Using morphological classifications from GZ1, Masters et al. (2010) found 6% of a sample of ∼5000 spirals to be red; similarly, Schawinski et al. (2009) found 6% of early-type galaxies to be blue. The existence of these objects may represent transition phases in the pathway from the blue cloud to the red sequence, and also give insight into what processes may quench or initiate star-formation without inducing a morphological change, or visa versa.

Another probe for understanding the transition from blue cloud to red sequence is the "green valley", the intermediate region between the two. In addition to the ellipticals in the blue cloud and spirals in the red sequence, galaxies of all types residing in the green valley were thought to represent the transition stages of this evolutionary pathway. The intermediate colors in this region indicate a recent quenching of star-formation (Martin et al. 2007; Salim et al. 2007), and the dearth of galaxies here (as compared to the high populations in the red sequence and blue cloud) initially suggested that the quenching process initiating transition across the CMD is very rapid.

A closer look at the populations within the green valley show that the processes causing galaxies to evolve from the blue cloud to red sequence may be very different. Schawinski et al. (2009) studied the morphological distribution (measured by the GZ1 project) of ∼4000 green-valley galaxies, finding that late-type and early-types likely go through two different evolutionary tracks. For late-types, the quenching process is gradual, and initiated by a cutoff of a gas reservoir. Galaxies quenched recently in this way would populate the green valley at $z = 0$, and those which quenched at an earlier time would be currently identified as red passive disks. Whether these red disks continue to evolve into spheroidals via some process after the initial quenching is unclear from a local Universe analysis. For early-types, the quenching is rapid and probably external and violent, thus triggering the morphological change from disk to spheroidal.

Analysis of the color-morphology relationship in the local Universe has revealed a close but imperfect bimodality as well as proposed mechanisms by which galaxies undergo different quenching processes, driving their evolution along the CMD. Even more may be revealed by studying the different populations as a function of cosmic time, which is becoming more possible with the data from large high-redshift surveys such as COSMOS and deep imaging via HST-ACS. It has been established now, for instance, that the bimodality does exist out to $z \sim 1$ (Bell et al. 2004; Cirasuolo et al. 2007; Mignoli et al. 2009) and possibly beyond (Giallongo et al. 2005; van Dokkum et al. 2006; Franzetti et al. 2007; Cassata et al. 2008). What requires further study is how exactly the proportions change at different epochs.

To add: summary of quenching mechanisms, color-morphology relationship at higher redshift

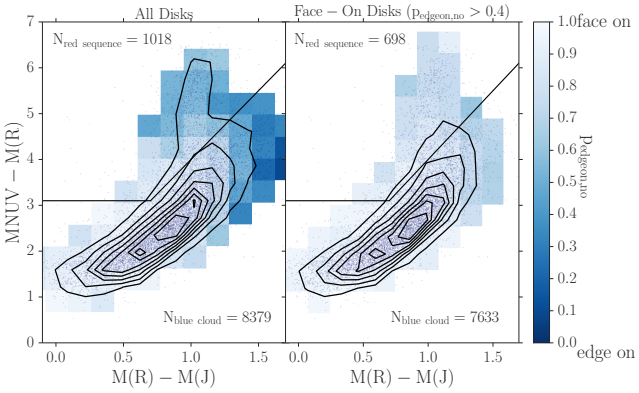

Figure 1.

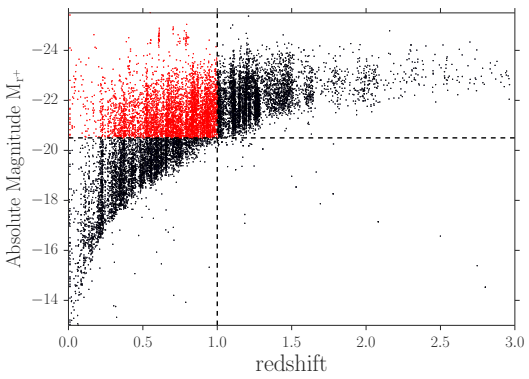

Figure 2. 70,198 COSMOS galaxies cross-matched in GZH and UltraVISTA (all points). 27,584 are in volume-limited sample (red points).

2 DATA

The parent sample of galaxies in this paper is drawn from the Galaxy Zoo: Hubble (GZH) catalog (Willett et al. 2016), which provides morphological classifications for galaxies sourced from the HST Legacy Surveys. From the main catalog we select galaxies with imaging from the Cosmic Evolution Survey (COSMOS, Scoville et al. (2007)) in the redshift range $0 < z < 1$. From this, we apply a magnitude cut of $M_{r^+} < -20.5$ to create a volume-limited sample. Rest frame NUV-r and r-J colors are taken from the UltraVISTA catalog (McCracken et al. 2012; Ilbert et al. 2013).

2.1 Selecting passive disk galaxies

We identify a sample of non-clumpy disk galaxies using the morphological classifications provided by GZH. The sample includes subjects which meet the following criteria: $f_{features} > 0.30$ and $f_{clumpy,no} > 0.30$, where f is the debiased vote fraction. We also require at least 20 votes for each question ($N_{smooth\ or\ features} \geqslant 20$ and $N_{clumpy} \geqslant 20$) to reduce uncertainty in the vote fractions.

To classify the galaxies as quiescent or star-forming, a method similar to that described by Ilbert et al. (2013) (hereafter I13) was used, which implements a rest-frame NUV-r^+ versus r^+-J diagnostic. Here are some reasons these colors are great (NUV-r:) (Arnouts et al. 2007; Salim et al. 2005; Wyder et al. 2007),(Martin et al. 2007)

The demarcation line to separate the quiescent and active populations at $z = 1$ is adopted from I13, which defines the quiescent galaxies as those which satisfy: $M_{NUV} - M_{r^+} > 3(M_{r^+} - M_J) + 1$ and $M_{NUV} - M_{r^+} > 3.1$. I13 applies this criteria to all galaxies in a range of $0.2 < z < 3$, although it performs best at separating the two populations in the redshift bin $0.7 < z < 1.2$, where $> 98\%$ of galaxies identified as quiescent exhibited star formation rates less than $log(SFR) = -11$ (see Figure 3 of I13). Therefore this work uses the I13 separation criteria at $z = 1$, and computes the evolution of the demarcation lines as a function of redshift to $z = 0$.

The evolution of $r-J$ and $NUV-r$ colors was measured using a stellar population synthesis model from Bruzual & Charlot (2003). An instantanious-burst model (ssp) was chosen from the Padova1994 track to represent the color evolution of a passively evolving galaxy, with a metallicity $Z = 0.008 = .4Z_{\odot}$, which is the typical metallicity of passive galaxies with mass $9 < log(M_*/M_{\odot}) < 10$ (Peng et al. (2015), Figure 2a), chosen to correspond to the median mass of the sample ($log(M_*/M_{\odot}) = 9.7$). A linear fit was geenerate for each color within the range $0 < z < 2$, and the slopes for each were used to redefine the demarcation lines in five redshift bins: one with central value $z = 0.007$ (used to classify the SDSS ferengi2 sample), and four with central values $z = [0.30,0.50,0.70,0.90]$ with widths $\Delta z = 0.2$. The quiescent galaxies are thus defined in these bins as those that satisfy:

$$M_{NUV} - M_{r^+} > 3.1 + a_1(z) \quad (1)$$

$$M_{NUV} - M_{r^+} > 3(M_{r^+} - M_J + a_2(z)) + a_1(z) + 1 \quad (2)$$

where $a_1(z) = [0.54, 0.38, 0.27, 0.16, 0.05]$ and $a_2(z) = [0.19, 0.14, 0.10, 0.06, 0.02]$.

3 CORRECTING FOR INCOMPLETENESS IN DISK DETECTION

In this work, we study the growth of the red sequence population by evaluating the fraction of passive disks as a function of redshift, $N_{red\ disks}/(N_{red\ disks} + N_{blue\ disks})$, as well as the fraction of disks occupying the red sequence, $N_{red\ disks}/(N_{red\ disks} + N_{red\ ellipticals})$. To accurately measure these fractions, the number of disks populating each redshift interval must be known with confidence. To identify disk galaxies in our sample, we set a cut of $f_{features} \geqslant 0.3$, such that galaxies meeting this criteria are considered to have distinguishable features or disk structure (additional cuts are also placed to eliminate clumpy, highly inclined, and merging galaxies; see Section 2.1). However, it is known that distinguishing disk structure from spheroidal becomes increasingly challenging at high redshifts (for both experts and novice classifiers alike), where features are less resolved and more difficult to identify. Willett et al. (2016) show using a set of artificially-redshifted simulated galaxy images classified in Galaxy Zoo that vote fractions for the same galaxy can be drastically different measured at $z = 1$ from

$z = 0$, often enough to change its morphological classification (we will show the same in Section 3.1). Therefore it is predicted that applying a $f_{\rm features}$ cut to identify disks will increasingly underestimate their true number at increasing redshift intervals. A set of artificially redshifted images was used to quantify and correct for this incompleteness in disk detection, described in the next section.

3.1 FERENGI2 set of artificially redshifted galaxy images

FERENGI2 is a set of simulated galaxy images created using the FERENGI code (Barden et al. 2008). These were created from a parent sample of 936 nearby ($z < 0.01$) SDSS galaxies, all of which had been previously classified in Galaxy Zoo 2 and were cross-matched in 2MASS (Skrutskie et al. 2006) for J magnitudes and GALEX (Martin et al. 2005) for NUV magnitudes, which were necessary to create a color-color separation using a method as similar as possible to that of the COSMOS sample. An evolution factor of $e = -1$ was applied, which brightens each galaxy linearly with redshift: $M' = M + ez$, where M' is the corrected magnitude. This correction is performed to mimic the known physical increase of galaxy magnitude with redshift (Lilly et al. 1998; Loveday et al. 2011), and the value $e = -1$ was chosen based on an analysis of spectra template models provided by Brinchmann et al. (2004), which showed that typical galaxies tend to evolve in brightness by one magnitude per redshift. Each galaxy was artificially redshifted 8 times from $z = 0.3$ to $z = 1$ in intervals of $\Delta z = 0.1$ and processed to mimic *HST* imaging parameters, giving a total of 7,488 images (3 examples are shown in Figure 4). The set was then classified in Galaxy Zoo using the same decision tree as used for Galaxy Zoo Hubble. 134 highly inclined disk galaxies were removed from the sample by excluding any with $N_{edgeon} > 20$ and $f_{not\ edge-on} >= 0.6$, using the vote fraction associated with the real galaxy image measured in GZ2. This cut was shown in Galloway et al. (2015) to correlate well with inclination angle $cos(a/b) < 67°$. This was to exclude those which may be mis-classified due to dust-reddening. Using the NUV-J-R selection method described in section 2.1, the remaining sample was divided into a set of red sequence galaxies (259 per redshift bin) and blue cloud (543 per each redshift bin) (see Figure 3).

3.2 Measuring ξ

The FERENGI2 set was used to measure the incompleteness in disk detection, from which a correction factor ξ was derived. This is defined as the number of disks detected divided by the true number of disks expected to exist in a given redshift interval: $\xi(z) = \mathrm{N_{detected}}/\mathrm{N_{true}}$. Acknowledging that the completeness in disk detection may depend on galaxy color, the corrected fraction of passive disks can then be calculated as:

$$f_{R|D} = \frac{N_{RD} \times \xi_{red}^{-1}}{N_{RD} \times \xi_{red}^{-1} + N_{BD} \times \xi_{blue}^{-1}} \qquad (3)$$

If there is no color bias in disk detection, $\xi_{red} = \xi_{blue}$, and this term cancels out, leaving the fraction unchanged. If there is a bias, however, the ξ terms do not cancel, and the incompleteness in disk detection could have a large effect on the red disk fraction. Therefore a careful measurment of ξ is estimated for both red and blue disk galaxies using the FERENGI2 set of simulated images.

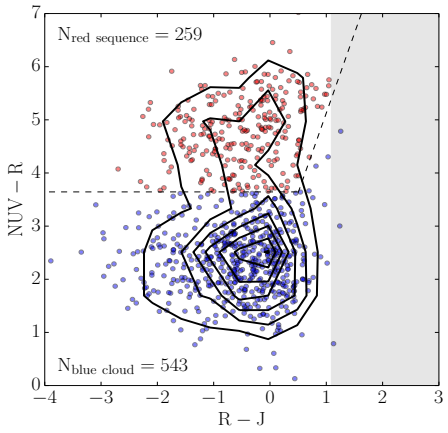

Figure 3. Separation of the quiescent population (red sequence) and active population (blue cloud) of the FERENGI2 sample. The gray shaded region represents the R-J limit of the sample; since FERENGI2 is a subset of GZ2, for which a limit of $r < 17$ was implemented, and the magnitude limit of 2MASS is $J < 15.91$, the FERENGI2 sample is limited to R-J < 1.1.

The completness values $\xi_{red}(z)$ and $\xi_{blue}(z)$ were computed in varying bins of redshift for the red sequence and blue cloud galaxies separately. An example calculation of ξ_{blue} in the $z = 0.7$ bin is shown in Figure 5. Each point represents a FERENGI2 galaxy, where the y-axis indicates the value of $f_{\rm features}$ measured in the image redshifted to $z = 0.7$, and the x-axis indicates the value of $f_{\rm features}$ measured in the same galaxy redshifted to $z = 0.3$. Disk galaxies are identified as those for which $f_{\rm features} \geqslant 0.3$. Since, on average, $f_{\rm features}$ decreases for the same galaxy as it is viewed at higher redshifts, the number of galaxies meeting this threshold is generally fewer at higher redshifts than lower redshifts. This is indicated by the dotted lines: galaxies to the right of the vertical dashed line at $\mathrm{f_{features,z=0.3}} = 0.3$ are identified as disks at $z = 0.3$; their sum is considered the "true" number of disks, $\mathrm{N_{true}}$. Similarly, the galaxies above the horizontal line at $\mathrm{f_{features,z=0.7}} = 0.3$ are identified as disks at $z = 0.7$; their sum is the "detected" number of disks at $z = 0.7$, or $\mathrm{N_{detected}}$. As obvious in the figure, $\mathrm{N_{detected}}$ is in general much lower than $\mathrm{N_{true}}$, emphasizing the increasing difficulty in detecting features at higher redshifts. Their ratio is the completeness ξ; in this example $\xi_{blue}(z = 0.7) = 0.61$, meaning only 61% of disks were detected at this redshift.

It was hypothesized that the completeness in disk detection may be a function of other parameters in addition to redshift. At fixed redshift, for example, it is reasonable to guess that features could be easier to detect galaxies that have higher mass, radius, or surface brightness. To test whether these parameters also impact the number of disks detected, the completeness was measured in fixed redshift bins as a function of surface brightness, effective radius, and mass. The surface brightness was calculated as

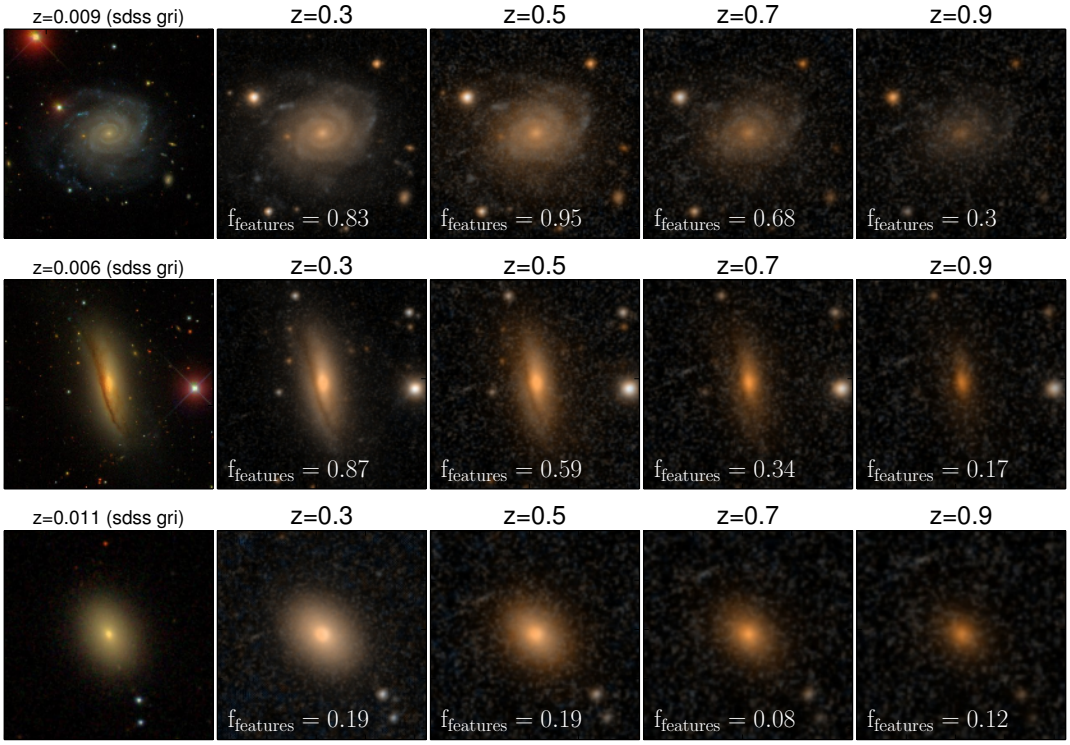

Figure 4. Example images of three galaxies artificially redshifted with the FERENGI code. The left image in each row is a real SDSS gri-composite image; the four to the right are images generated by FERENGI at varying redshifts, processed to mimic *HST*/*COSMOS* imaging. The $f_{\rm features}$ vote fraction for each simulated image is given; this value tends to decrease for each galaxy as it is processed to be viewed at higher redshifts.

$\mu = m + 2.5 * \log_{10}(2 \times (b/a) \times \pi R_e^2)$, using SExtractor outputs `MAG_AUTO`, b/a and R_e measured in the I_{814W} band images. The effective radius used was the 50% `FLUX_RADIUS` converted in to kpc, and the masses used were the `MEDIAN` values in the MPA-JHU DR7 catalog (Kauffmann et al. 2003).

Figure 6 shows completeness as a function of redshift and surface brightness, for the red sequence and blue cloud galaxies. 8 redshift bins were further divided into bins of surface brightness with varying widths, where the sizes were chosen to satisfy that $\rm N_{detected} + N_{true} \geqslant 10$ in each bin. This was chosen as a comprimise between having a sufficient number of galaxies in each bin to compute the completness fraction $\xi = \rm N_{detected}/N_{true}$, and to have enough bins of surface brightness to measure a trend with confidence of completeness as a function of μ. Visual inspection of the data did not suggest any relationship between the two. To be sure, the data were fit to a linear function in each redshift bin. For each fit, a p-value representing a hypothesis test whose null hypothesis is that the slope is zero was computed. Only one reached the criteria $p < 0.05$, but with a low R^2 value of 0.28 which is not considered large enough to represent a good fit. This process was repeated using effective radius and mass as parameters, with the same results. Therefore only redshift was used as a parameter which impacted completeness value with confidence.

The completeness values $\xi_{\rm red}$ and $\xi_{\rm blue}$ were then measured as a function of redshift for the red sequence and blue cloud FERENGI2 galaxies; results are shown in Figure 7. No significant difference was detected for the two functions, which is apparent from the overlapping $1-\sigma$ errors on the plot. Therefore ξ was computed for all galaxies in bins of redshift between 0.3 and 1.0 with widths $\Delta z = 0.1$; from here a linear relationship for ξ as a function of redshift was derived: $\xi(z) = -0.9 \pm x(z) + 1.2 \pm y$. This correction was used to calculate the fraction of disks on the red sequence:

$$f_{D|R} = \frac{N_{RD} \times \xi^{-1}(z)}{N_{RD} + N_{RE}} \quad (4)$$

4 RESULTS

In this section we present our results of the evolution of disc galaxies from $z = 1$ to $z = 0.2$ in a sample of 27,355 *COSMOS* galaxies morphologically classified in GZH. We will show x, y, and z and talk about it.

4.1 The evolving passive disk fractions: $f_{R|D}$ and $f_{D|R}$

The change in the relative number densities of active/passive disk/elliptical galaxies traces the dominant evolutionary pathways they follow at different mass thresholds. In Figure 8 we measure these using the fractions defined in the previous section, $f_{R|D}$ (left panel) and $f_{D|R}$ (right panel) for

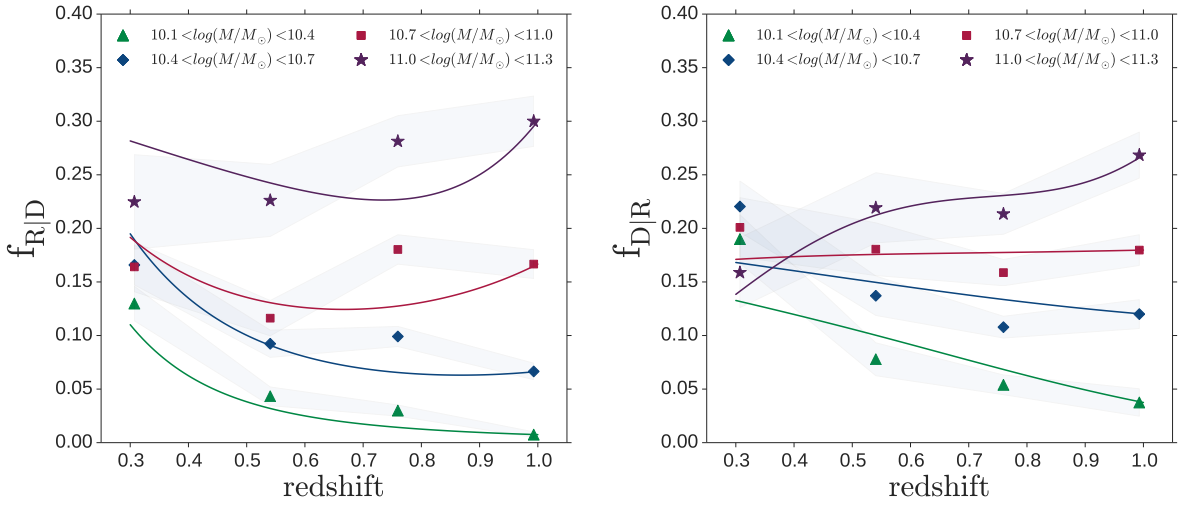

Figure 8. Left: Passive disk fraction ($N_{red\ disks}/(N_{red\ disks} + N_{blue\ disks})$) vs redshift in four mass bins. **Right:** Fraction of disks on the red sequence ($N_{red\ disks}/(N_{red\ disks} + N_{red\ ellipticals})$) vs redshift in four mass bins.

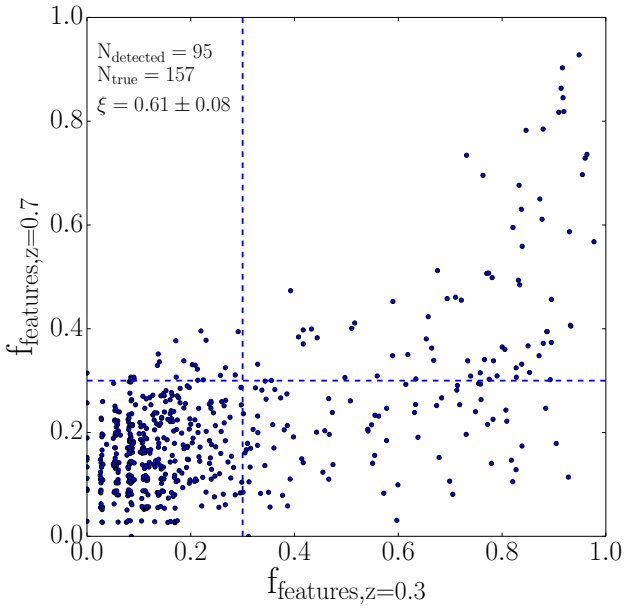

Figure 5. Example calculation of completeness ξ at redshift $z = 0.7$. Points represent FERENGI2 images classified in Galaxy Zoo. The y-axis corresponds to the value of $f_{features}$ measured at the galaxy redshifted to $z = 0.7$, and the x-axis corresponds to the value of $f_{features}$ measured at the galaxy redshifted to $z = 0.3$. On average, the $f_{features}$ is lower at the higher redshift, indicating users on average have more difficulty identifying features in images at higher redshifts. The dotted lines correspond to $f_{features}$=0.3, the threshold above which a galaxy is considered to have a disk. Galaxies to the right of the vertical dashed line were identified as disks at the lowest redshift $z = 0.3$, the total number defined as N_{true}, the true number of disks. Galaxies above the horizontal dash line were identified as disks at the higher redshift $z = 0.7$, the total number defined as $N_{detected}$. The ratio $\xi = N_{detected}/N_{true}$ is the completeness value; in this example, only 61% of disks were detected at $z = 0.7$.

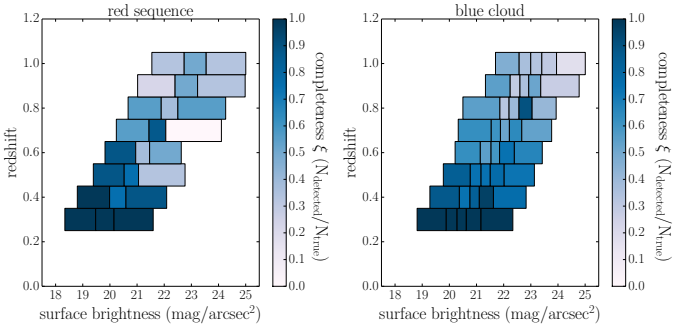

Figure 6. Completeness ξ as a function of redshift and surface brightness for red sequence (left) and blue cloud galaxies (right). In each redshift bin, galaxies were binned by surface brightness in varying widths such that $N_{detected} + N_{true} \geqslant 10$ in each bin. The completeness ξ was computed in each z, μ bin, represented by the colors. Darker colors represent a completeness of 1, such that all disks were detected, while fainter colors represent a completeness near 0, representing a failure to detect disks. ξ tends to decrease with redshift, but no correlation of ξ with surface brighness is observed at fixed redshift.

four mass bins. We observe significantly different trends in $f_{R|D}$ for the two highest mass bins ($log(M/M_\odot) > 10.7$): for higher-mass galaxies, the fraction of red disks vs. all disks, within error, is either relatively flat or exhibits a small decrease, while the lower-mass galaxies have trends which increase sharply from $z = 1$ to $z = 0.3$. Similarly for the fraction of red disks on the red sequence: the highest mass bin $log(M/M_\odot) > 11.0$ decreases in $f_{D|R}$, while the lowest-mass bin increases sharply from $f_{D|R} \sim 0.05$ to ~ 0.2.

To gain a more intuitive understanding of how the trends of these fractions depend on the different possible evolutionary pathways and their transition rates, it is helpful to rewrite them in a reduced form: $f_{R|D} = (1 + \frac{N_{BD}}{N_{RD}})^{-1}$; $f_{D|R} = (1 + \frac{N_{RE}}{N_{RD}})^{-1}$. Using the former as an example: at zeroth order, it can be seen that if the number of red disks increases at a higher rate than an increase in blue disks

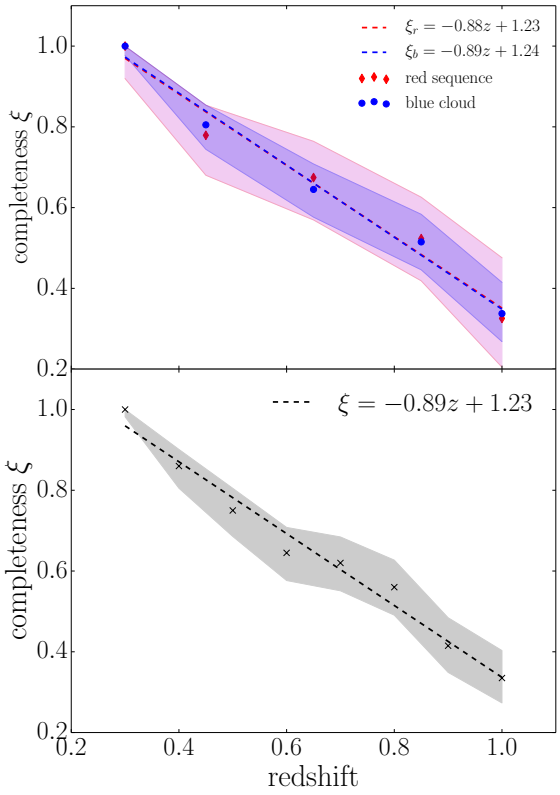

Figure 7. Top: Completeness ξ as a function of redshift for red sequence and blue cloud FERENGI2 galaxies separately. Both populations show a strong dependence on ξ with redshift, but are indistinguishable from each other. **Bottom:** Completeness as a function of redshift for all FERENGI2 galaxies (red and blue combined). The equation representing the linear fit is displayed.

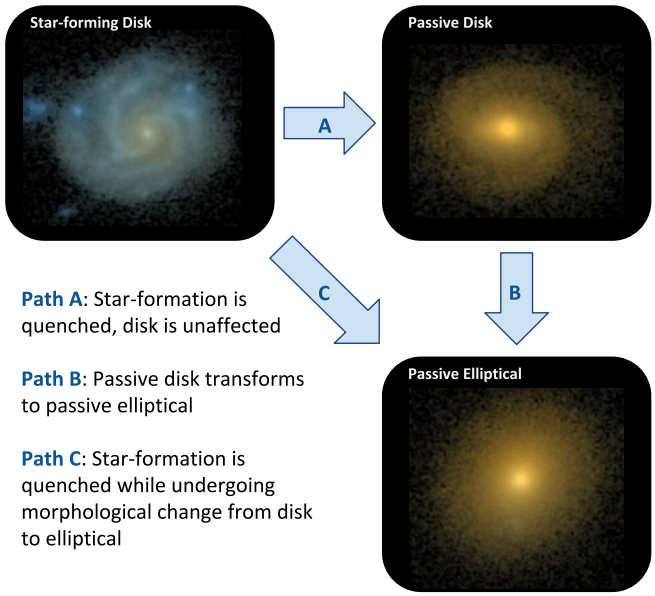

Figure 9. cartoon

in some time interval, the overall fraction $f_{R|D}$ would also increase. For a single mass bin, this scenario would be consistent with a model in which blue galaxies are quenching faster than they are entering the mass bin via star formation. A strong decrease in $f_{R|D}$ would, in constrast, indicate a higher rate of red disks exiting the mass bin than the blue disks; the strength of the decrease would depend on the relative frequencies of blue galaxies quenching to form new red disks and red disks merging to form red ellipticals. The precise relative values of these rates cannot be deduced by a simple by-eye analysis of the fraction, however.

We therefore implement a simple toy model to track the change in $f_{R|D}$ and $f_{D|R}$, given a range of parameters representing the quenching and morphological transformation rates for galaxies at fixed stellar mass. We begin by considering the rate of change in the number of blue disks (dN_{BD}/dt), red disks (dN_{RD}/dt), and red ellipticals (dN_{RE}/dt). In a given mass bin, the change in numbers for each population will depend on several parameters, illustrated visually in Figure 9.

4.1.1 Blue Disks

First, galaxies in a blue bin may transition into a red disk bin via a quenching process that does not destroy its disk; we define this rate as $r_{BD\rightarrow RD}$, representing the fraction of blue galaxies to transition to red disks per Gyr (path A in Figure 9). Blue galaxies may also exit a bin via a quenching process which *does* destroy the disk; this fraction per Gyr we define as $r_{BD\rightarrow RE}$ (path C in Figure 9).

The number of galaxies in a blue disk bin will also change due to star formation, which brings active galaxies from a lower mass bin into the current mass bin. To account for this term we use the formalism outlined by Peng et al. (2010), in which this rate of change is given by $(\alpha + \beta)sSFR$. Here $\alpha = d\phi_{blue}/dm$ is the derivative of the mass function for blue galaxies, which equates to $\alpha = (1 + \alpha_s) - m/M^*$ for a mass function described by the Schechter (1976) function. We use best-fit parameters for blue galaxies measured by Johnpaperetal, which give $\alpha_s = -1.4$ and $M^* = 10.28$ ($log(M/M_\odot)$). Following the method of Peng et al. (2010), we let $\beta = 0$, both for simplicity, and because their conclusions found not to be strongly dependent on β. Last, the specific star-formation rate is given by $sSFR(t) = 2.5(\frac{t}{3.5Gyr})^{-2.2}Gyr^{-1}$ (Peng et al. 2010).

Accounting for all sources and sinks of blue disks entering or exiting a bin of given mass, the rate of change of blue disks can be written fully as:

$$\frac{dN_{BD}}{dt}\Big|_m = \Big(-r_{BD\rightarrow RD} - r_{BD\rightarrow RE}\Big)N_{BD} - \alpha(m)sSFR(t) \quad (5)$$

4.1.2 Red Disks

Galaxies exiting a blue bin as they quenched without disrupting their disks enter the pool of red disks, increasing N_{RD} for a given mass bin. Red disks also may undergo a morphological transformation, depleting the pool of red disks as they enter the red elliptical bin (path B in Figure 9). The fraction of galaxies to undergo this pathway per

Gyr is denoted as $r_{RD->RE}$. Combining these factors gives the expression:

$$\frac{dN_{RD}}{dt}\Big|_m = +r_{BD\rightarrow RD}N_{BD} - r_{RD\rightarrow RE}N_{RD} \quad (6)$$

4.1.3 Red Ellipticals

In this simple model, it is assumed that red, passive ellipticals are the final state in a typical galaxy's evolution. Therefore N_{RE} will always be increasing from the transformation from blue disks and red disks to red ellipticals ($r_{BD\rightarrow RE}$, $r_{RD\rightarrow RE}$). However, the number of red ellipticals *in a single mass bin* may still decrease due to ellipticals at the given mass merging to enter a bin of red ellipticals at a higher mass. Similarly, their number can increase as ellipticals from a lower mass bin merge to enter the current mass bin. A complete, semi-analytic model would consider this full range of possibilities and couple the resulting equations appropriately amongst all mass bins. For the purposes of this simple model, we opted to represent the total, net rate of change of the number of red ellipticals as a single parameter, κ_{RE}, which we note may be positive or negative, depending on whether more ellipticals are entering or leaving the given mass bin.

$$\frac{dN_{RE}}{dt}\Big|_m = \kappa_{RE}N_{RE} \quad (7)$$

We initialize our model using the observed relative numbers of blue disks, red disks, and red ellipticals measured at $z = 1$, then use the model to compute their evolution to $z = 0.3$ using a range of values for each of the four parameters in four mass bins. For $r_{BD\rightarrow RD}$, $r_{BD\rightarrow RE}$, and $r_{RD\rightarrow RE}$, we test 25 values between 0 and 1, and 25 values between -1 and 1 for κ_{RE}. We note that a complete model would explore time-varying rates, but for the purposes of simplicity in our toy-model we only experiment with static parameters. For each mass bin, the model was implemented for each permutation of the four rate parameters. The success of each run was evaluated using a χ^2 metric; these results are shown for each mass bin in the corner-plot in Figure 10. The bins are weighted by $1/\chi^2$, such that white regions represent the rate parameters that yield the lowest χ^2, and black representing the largest.

We find a strong mass dependence on the fraction of blue galaxies to quench to red disks ($r_{BD\rightarrow RD}$), or Path A in Figure 9. Our observations of $f_{R|D}$ and $f_{D|R}$ are most closely reproduced when $r_{BD\rightarrow BD}$ = [0.05, 0.1, 0.15, 0.2] Gyr^{-1} for masses log(M/M$_\odot$) = [10.25,10.55,10.85,11.0]. These values for $r_{BD\rightarrow RD}$ correspond to the peaks of the 1-D histograms shown in Figure 10.

5 DISCUSSION

6 CONCLUSIONS

The data in this paper are the result of the efforts of the Galaxy Zoo Hubble volunteers, without whom none of this work would be possible. Their efforts are individually acknowledged at `authors.galaxyzoo.org`. Please contact the author(s) to request access to research materials discussed in this paper.

MG, CS, MB, and LF gratefully acknowledge support from the US National Science Foundation Grant AST1413610.

This publication makes use of data products from the Two Micron All Sky Survey, which is a joint project of the University of Massachusetts and the Infrared Processing and Analysis Center/California Institute of Technology, funded by the National Aeronautics and Space Administration and the National Science Foundation.

This project made heavy use of the Astropy packages in Python (Robitaille et al. 2013), the `seaborn` plotting package (Waskom et al. 2015), and the Tool for OPerations on Catalogues And Tables (TOPCAT), which can be found at `www.starlink.ac.uk/topcat/` (**?**).

Funding for the SDSS and SDSS-II has been provided by the Alfred P. Sloan Foundation, the Participating Institutions, the National Science Foundation, the U.S. Department of Energy, the National Aeronautics and Space Administration, the Japanese Monbukagakusho, the Max Planck Society, and the Higher Education Funding Council for England. The SDSS website is `http://www.sdss.org/`.

The SDSS is managed by the Astrophysical Research Consortium for the Participating Institutions. The Participating Institutions are the American Museum of Natural History, Astrophysical Institute Potsdam, University of Basel, University of Cambridge, Case Western Reserve University, University of Chicago, Drexel University, Fermilab, the Institute for Advanced Study, the Japan Participation Group, Johns Hopkins University, the Joint Institute for Nuclear Astrophysics, the Kavli Institute for Particle Astrophysics and Cosmology, the Korean Scientist Group, the Chinese Academy of Sciences (LAMOST), Los Alamos National Laboratory, the Max-Planck-Institute for Astronomy (MPIA), the Max-Planck-Institute for Astrophysics (MPA), New Mexico State University, Ohio State University, University of Pittsburgh, University of Portsmouth, Princeton University, the United States Naval Observatory and the University of Washington.

REFERENCES

Arnouts S. et al., 2007, Astronomy and Astrophysics, 476, 137

Baldry I. K., Glazebrook K., Brinkmann J., Ivezić Ž., Lupton R. H., Nichol R. C., Szalay A. S., 2004, The Astrophysical Journal, 600, 681

Barden M., Jahnke K., Häußler B., 2008, The Astrophysical Journal Supplement Series, 175, 105

Bell E. F. et al., 2004, The Astrophysical Journal, 608, 752

Brinchmann J., Charlot S., White S. D. M., Tremonti C., Kauffmann G., Heckman T., Brinkmann J., 2004, Monthly Notices of the Royal Astronomical Society, 351, 1151

Bruzual & Charlot, 2003, Monthly Notices of the Royal Astronomical Society, 344, 1000

Cassata P. et al., 2008, Astronomy and Astrophysics, 483, L39

Cirasuolo M. et al., 2007, Monthly Notices of the Royal Astronomical Society, 380, 585

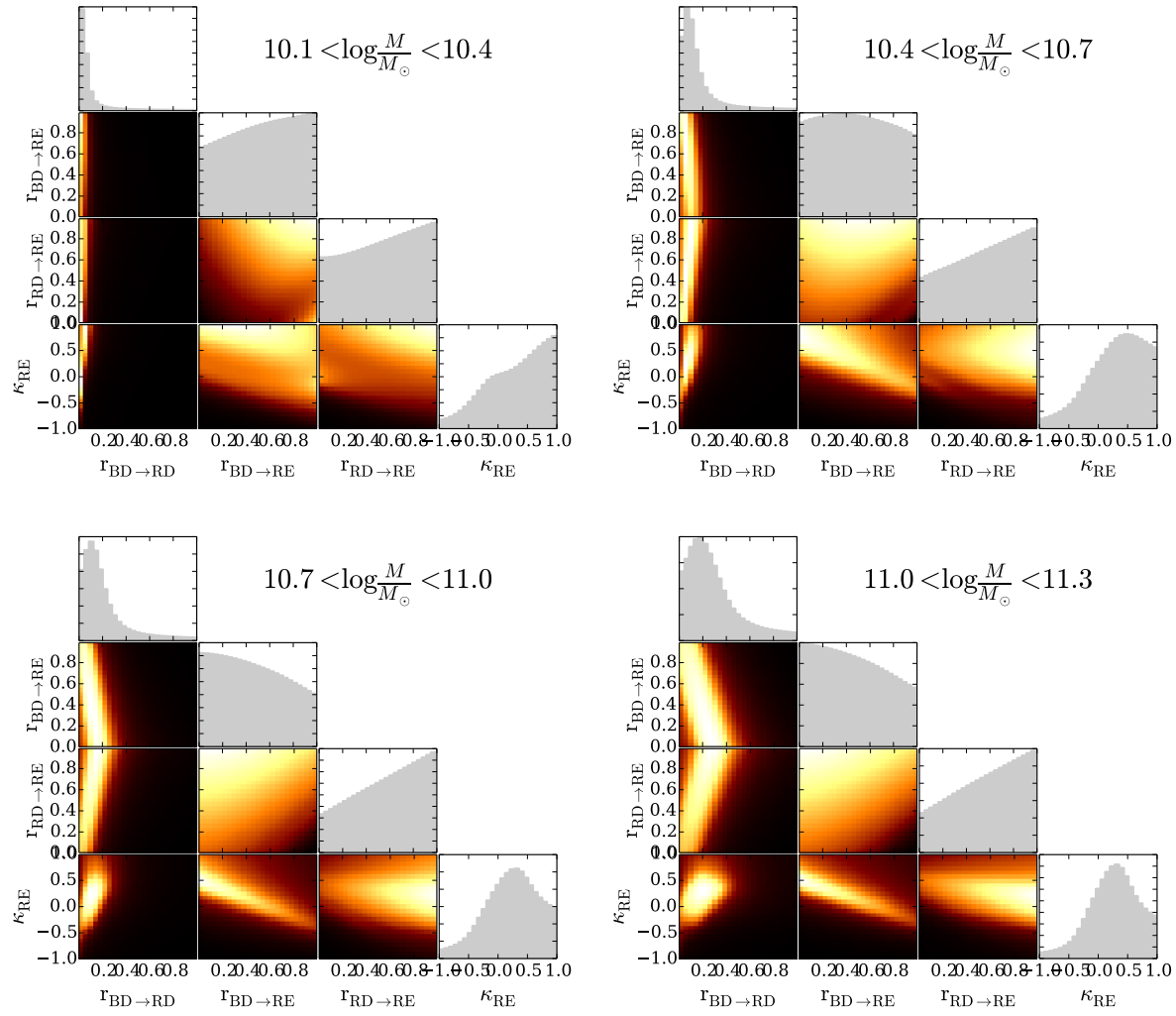

Figure 10. The units for all rate parameters is Gyr^{-1}.

Cooray A., 2005, Monthly Notices of the Royal Astronomical Society, 363, 337
Correa C. A., Schaye J., Clauwens B., Bower R. G., Crain R. A., Schaller M., Theuns T., Thob A. C. R., 2017
Franzetti P. et al., 2007, Astronomy and Astrophysics, 465, 711
Galloway M. A. et al., 2015, Monthly Notices of the Royal Astronomical Society, 448, 3442
Giallongo E., Salimbeni S., Menci N., Zamorani G., Fontana A., Dickinson M., Cristiani S., Pozzetti L., 2005, The Astrophysical Journal, 622, 116
Ilbert O. et al., 2013, Astronomy & Astrophysics, 556, A55
Kauffmann G. et al., 2003, Monthly Notices of the Royal Astronomical Society, 341, 54
Lee J., Pen U.-L., 2007, The Astrophysical Journal, 670, L1
Lilly S. et al., 1998, The Astrophysical Journal, 500, 75
Loveday J. et al., 2011
Martin D. C. et al., 2005, The Astrophysical Journal, 619, L1
Martin D. C. et al., 2007, The Astrophysical Journal Supplement Series, 173, 342
Masters K. L. et al., 2010, Monthly Notices of the Royal Astronomical Society, 405, 783
McCracken H. J. et al., 2012, Astronomy & Astrophysics, 544, A156
Mignoli M. et al., 2009, Astronomy and Astrophysics, 493, 39
Peng Y., Maiolino R., Cochrane R., 2015, Nature, 521, 192
Peng Y.-j. et al., 2010, The Astrophysical Journal, 721, 193
Robitaille T. P. et al., 2013, Astronomy & Astrophysics, 558, A33
Salim S. et al., 2005, The Astrophysical Journal, 619, L39
Salim S. et al., 2007, The Astrophysical Journal Supple-

ment Series, 173, 267
Salimbeni S. et al., 2008, Astronomy and Astrophysics, 477, 763
Schawinski K. et al., 2009, The Astrophysical Journal, 690, 1672
Scoville N. et al., 2007, in AIP Conference Proceedings, Vol. 943, AIP, pp. 221–228
Simon P., Hetterscheidt M., Wolf C., Meisenheimer K., Hildebrandt H., Schneider P., Schirmer M., Erben T., 2009, Monthly Notices of the Royal Astronomical Society, 398, 807
Skrutskie M. F. et al., 2006, The Astronomical Journal, 131, 1163
Strateva I. et al., 2001, The Astronomical Journal, 122, 1861
van Dokkum P. G. et al., 2006, The Astrophysical Journal, 638, L59
Waskom M. et al., 2015
Willett K. W. et al., 2016, 32
Wyder T. K. et al., 2007